# Toggling of seismicity by the 1997 Kagoshima earthquake couplet: A demonstration of time-dependent stress transfer

Shinji Toda
Active Fault Research Center, Geological Survey of Japan, AIST

Ross Stein
U.S. Geological Survey, Menlo Park, California

**Abstract**. Two **M**~6 well-recorded strike-slip earthquakes struck just 4 km and 48 days apart in Kagoshima prefecture, Japan, in 1997, providing an opportunity to study earthquake interaction. Aftershocks are abundant where the Coulomb stress is calculated to have been increased by the first event, and they abruptly stop where the stress is dropped by the second event. This ability of the mainshocks to toggle seismicity on and off argues that static stress changes play a major role in exciting aftershocks, whereas the dynamic Coulomb stresses and earthquake shaking—which should only excite seismicity—can play a minor role. If so, one would expect that the net stress changes from an earthquake sequence would forecast the subsequent seismicity distribution. But adding the stress changes from the two Kagoshima events does not fully capture the ensuing seismicity, such as its temporal decay in rate or its migration away from the ends of the ruptures. We therefore implement a stress transfer model that incorporates rate/state friction, in which seismicity is treated as a sequence of independent nucleation events in which the state depends on the fault slip, slip rate, and elapsed time since the last event. The model reproduces the temporal response of seismicity to successive stress changes, including toggling, decay, and aftershock migration. Nevertheless, the match of observed to predicted seismicity is quite imperfect, perhaps because of inadequate knowledge of the background seismicity. We build a probabilistic forecast of larger earthquakes on the modeled rate of small aftershocks, taking advantage of the large statistical sample the small shocks afford. Not surprisingly, such probabilities are highly time and location-dependent: During the first decade after the mainshocks, the seismicity rate and the chance of successive large shocks is about an order of magnitude higher than the background rate, and is concentrated exclusively in the stress triggering zones.

## 1. Introduction

A principal tenet of the Coulomb hypothesis is that stress increases promote fault failure, while stress decreases inhibit failure. But the stress changes alone cannot explain the time behavior of seismicity, such as the universally observed Omori decay of aftershocks. When the Coulomb hypothesis is modified to incorporate the effects of rate/state friction [*Dieterich*, 1994], a sudden Coulomb stress increase causes a large increase in seismicity rate, but decays back toward its initial rate inversely with time. A sudden stress drop causes the seismicity rate to plummet, which also recovers towards its initial rate. In what we refer to as 'rate/state stress transfer,' the evolution of seismicity depends not only on the stress change and the static friction coefficient, but also on the background seismicity rate, a fault constitutive parameter, and either the fault stressing rate or an aftershock decay period. At the cost of additional parameters, rate/state stress transfer offers the prospect of more accurate seismicity forecasts.

Some progress has been achieved in demonstrating rate/state stress transfer in seismicity. Aftershocks located off the main fault rupture have proven the most useful tests of the concept. But if there are weaknesses in such studies, they stem from the difficulty of measuring seismicity rate declines, which requires that the background seismicity rate before the perturbing earthquake be quite high. Earthquakes in which stress decreases, or 'stress shadows,' have been associated with seismicity rate decreases include the 1989 **M**=6.9 Loma Prieta [*Parsons et al.*, 1999; *Reasenberg and Simpson*, 1997; *Stein*, 1999], 1906 **M**=7.9 San Francisco [*Harris and Simpson*, 1998], 1995 **M**=6.9 Kobe [*Toda et al.*, 1998], and 1992 **M**=7.3 Landers [*Wyss and Wiemer*, 2000] events; and along the Parkfield section of the San Andreas fault after the 1983 **M**=6.7 Coalinga earthquake [*Toda and Stein*, 2002].

A more convincing demonstration of rate/state stress transfer demands a case in which an off-fault region is subjected to alternating stress increases and decreases—toggling stress changes. Such a case is also valuable because one can test whether instead the dynamic and shaking effects of earthquakes are principally responsible for aftershocks and subsequent seismicity. In the 1997 Kagoshima sequence, the March 26 **M**=6.1 and May 13 **M**=6.0 mainshocks ($M_{JMA}$ 6.5 and 6.3, respectively) struck close together in time and space (Figure 1). The geometrical simplicity of the earthquakes, coupled with the quality of the seismic, strong motion, and geodetic data provide an opportunity to subject rate/state stress transfer to a more powerful test. We will argue that the common

practice of adding the Coulomb stress of two or more successive earthquakes to predict the resulting seismicity pattern (e.g., *Stein et* al. [1997], *Nalbant et al*. [1998], and *Hubert-Ferrari et al*. [2000]) is inferior to a rate/state stress transfer model.

## 2. Data

The 1997 earthquakes struck on three unmapped faults in a region of Kyushu Island with few known active faults and a low rate of historical seismicity. The Philippine Sea Plate subducts beneath southern Kyushu along the Nankai Trough at a rate of ~40 mm/yr (Figure 1, inset). Unlike Shikoku Island and other inland regions adjacent to the Nankai Trough, southern Kyushu is undergoing NW-SE extension [*Sagiya et al.*, 2000]. Most shallow earthquakes are strike-slip, and several active volcanoes and calderas align with a N-S trending volcanic front. No large destructive earthquake has struck within 75 km of the 1997 Kagoshima epicenters since records were kept starting in AD 679; the largest shock within 30 km is a 1994 $M_{JMA}$= 5.7 event that occurred 15 km to the northeast [*Earthquake Research Committee*, 1998; *Miyamachi et al*., 1999] (Figure 1). In the 1997 sequence produced left-lateral slip on two E-W planes and right-lateral slip on a N-S plane, with the ruptures oriented about 45° to the strike of the extensional strain. The Harvard CMT mainshock focal mechanisms indicate nearly pure strike-slip faulting on vertical faults. From strong motion analysis, *Horikawa* [2001] found a seismic moment of 1.6 x $10^{18}$ Nm for the March 26 event, with unilateral westward or bilateral rupture propagation. For the May 13 mainshock, he found a moment of 1.0 x $10^{18}$ Nm on two orthogonal faults, with rupture initiating near their junction. Variable slip models for both events from *Horikawa* [2001] are shown in Figure 2. The general features are consistent with independent InSAR and continuous GPS analysis of the March event by Fujiwara et al. [1998]. The asperity model of *Miyake et al.* [1999] also resembles Horikawa's slip distributions.

To study the response of seismicity to stress changes imparted by the Kagoshima shocks, one must measure the background seismicity rate before 26 March 1997 at the minimum magnitude of completeness, $M_c$. This is the magnitude at which the catalog is complete for a given period. If earthquakes with magnitudes below $M_c$ were included, there would be an apparent increase in seismicity following the mainshock because seismic stations that are typically added after a large mainshock enhance detection [*Matthews and Reasenberg*, 1988; *Wiemer and Wyss*, 2000]. Both the national Japan Meteorological

Agency (JMA) and local Kagoshima University (KU) [*Miyamachi et al.*, 1999] catalogs are available (Figure 3). *Miyamachi et al*. [1999] relocated the Kagoshima University catalog events in a 3-D P-wave velocity model inverted from travel times of 14 stations; $M_c$=0.9 during March 1996-March 2001 (Figure 4). JMA augmented its network in October 1994, after which $M_c$=2.2. While the lower $M_c$ and improved locations for the Kagoshima University data make it a better choice, $M_{KU}$=0.9 is roughly equivalent to $M_{JMA}$=1.6, so the disparity between the catalogs is smaller than it would appear (Figure 3).

## 3. Coulomb Stress Changes

*Mainshock triggering*. We first examine the interaction of the three largest shocks. We calculate that the 1994 $M_{JMA}$= 5.7 earthquake brought the March 1997 rupture 0.2-0.5 bars closer to Coulomb failure closer to failure, if the friction coefficient is as high as 0.8. This inference is consistent with the presence of off-fault aftershocks in the northern and southern triggering lobes of the 1994 shock; seismicity extends to the future 1997 fault plane (Figure 1). For low values of friction, however, the effects of the 1994 shock are negligible at the 1997 epicenters. *Parsons et al*. [1999] found that seismicity associated with faults with little cumulative slip is favored more by unclamping than shear, and thus young or low-slip-rate faults such as these may exhibit higher fault friction. The absence of a mapped fault in the 1997 events would suggest little cumulative slip, and so a high value of friction ($\mu$~0.8) may indeed be appropriate.

Whether the March shock brought the faults that ruptured in May closer to Coulomb failure is ambiguous, because it is not known which of the two orthogonal faults ruptured first in the May event. The stress change associated with the March rupture is resolved on the May faults in Figure 5. The shear stress change is negative except near the ground surface, whereas the normal stress unclamps both faults within 3 km of their junction, as previously reported by *Horikawa* [2001]. Thus only for high values of friction ($\mu \geq 0.8$) would the Coulomb stress promote failure, in which case the stress increase could have been as high as 5 bars at the fault junction. The May hypocenter may lie on the E-W fault (Kagoshima University location) or at the fault junction (JMA location). Only if the more strongly unclamped N-S fault ruptured first would the E-W rupture be subsequently unclamped. Although *Miyake et al.* [1999] found that the N-S fault

ruptured several seconds before the E-W rupture, *Horikawa* [2001] concluded the opposite, so our triggering conclusions are uncertain.

*Aftershock triggering*. Our principal focus is not on the several main shocks, but on the thousands of off-fault aftershocks, because they provide a large statistical sample. The top panels of Figure 6 show the Coulomb stress change associated with the March rupture, together with seismicity during the intervening 48 days before the May shock. The stress change associated with the May rupture, with the ensuing 48 days of seismicity, is shown in the middle panels of Figure 6c. The cumulative stress changes imparted by both earthquakes are shown in the lower panels of Figure 6. We set $\mu$=0.0 on the left panels, and $\mu$=0.8 on the right panels, of Figure 6. We resolve the Coulomb stress on strike-slip faults parallel to the main E-W ruptures. Focal mechanisms of M≥3 aftershocks appear consistent with this assumption, exhibiting near-vertical nodal planes striking parallel to the mainshock ruptures (Figure 7). We exclude from consideration earthquakes within 3 km of the fault ruptures (comprising 75% of the total), which we regard as arising from small-scale slip discontinuities and secondary fault fractures that are not represented by the smooth, planar slip model. For both the March and May stress changes, regions of concentrated off-fault aftershocks correspond to sites of calculated stress-increase, whereas off-fault aftershocks are rare in the stress shadows.

Although the correspondence between off-fault stress change and seismicity is good, there are features in the seismicity that cannot be explained by the stress changes alone. In Figure 8, we plot the daily rate of earthquakes in three off-fault boxes, marked A-C in Figure 6. These are sites off the mainshock rupture planes, where stress is calculated to have changed by more than 0.3 bars during each mainshock. Here we use $\mu$=0.8 on the basis of the inferred mainshock triggering and youth of the faults. Note that in most cases, the seismicity rate changes by orders of magnitude after each mainshock, whereas the stress change is never more than 4 bars. Boxes A and B were subjected to roughly the same net stress change (1.8 and 1.9 bars, respectively), yet the post-May seismicity rate is five times higher in box B (3.0 shocks/day) than in box A (0.6 shock per day). Neither these disparities, nor the Omori-like inverse-time decay in the seismicity rate after the March event in box A, can be explained by adding the static Coulomb stress changes, encouraging us to seek a more comprehensive model.

**4. Rate/State Stress Transfer**

To consider successive stress changes associated with multiple mainshocks, we use the expression for seismicity rate $R$ as a function of the state variable $\gamma$ from *Dieterich* [1994] (Figure 9). In the absence of a large stress perturbation, the seismicity rate is assumed constant (eqn 1 in Figure 9). The seismicity rate is altered by a stress step. A key element of rate/state friction theory is a nonlinear dependence of the time to instability on stress change. The effect of the stress increase on a fault is to cause $\gamma$ to drop, so the fault slips at a higher rate, causing a higher rate of seismicity (eqn 2). Conversely, a sudden stress drop lowers the rate of seismicity. But the seismicity rate change is transient and eventually recovers. The duration of the transient is inversely proportional to the fault stressing rate (eqn 3). Thus, given sufficient time (e.g., decades to centuries), the effect of all but the largest of earthquakes disappears. A critical feature of rate/state stress transfer is that the background seismicity rate before each shock plays a profound role on the effect of the coseismic stress change: the higher the background rate, the more a stress change amplifies the seismicity rate. If, on the other hand, the background rate is low, the stress changes have a muted effect on seismicity [*Marone*, 2002; *Toda et al.*, 2002]. Thus, two sites that sustain the same jump in stress can produce different increases in seismicity rate, as seen at Kagoshima.

*Rate/state algorithm*. The seismicity rate equation is implemented in the following manner: At the time of a mainshock, the updated value of $\gamma$ is used in eqn 2 (Figure 9), which then decays with time following eqn 3. When the next earthquake occurs, eqn 2 is used again with the latest value of $\gamma$. To evaluate terms in the equations, the Coulomb stress change is calculated for individual mainshocks, and $r$ is estimated from the background seismicity rate before the first mainshock in the sequence. The parameter, $A\sigma$, is the product of a constitutive parameter times the total normal stress; it describes the instantaneous response of friction to a step change in slip speed. We assume $A\sigma$ = 0.4 bar, based on the stress-change dependence of seismicity rate at the site of the 1995 Kobe earthquake [*Toda et al.*, 1998], another large strike-slip event in inland Japan. Similar estimates have been determined by *Guatteri et al*. [2001] for the Kobe shock ($A\sigma$ = 0.6 bar), and by *Belardinelli et al.* [1999] for the 1980 **M**=6.9 Irpinia, Italy, earthquake ($A\sigma$ = 0.8-0.9 bar). Given laboratory values of $A$ [*Dieterich*, 1994], these values of $A\sigma$ imply that the effective normal stress $\sigma$ is low (5-20 bars).

The background seismicity rate $r$ before the Kagoshima sequence is the most uncertain parameter, because the seismic catalogs have limited periods at the requisite low magnitudes of completion. The Kagoshima University catalog includes only one year before 26 March 1997 shock complete to M=0.9. From this we estimate a spatially uniform rate of 0.09 km$^{-2}$ yr$^{-1}$ (162 events in the 1820 km$^2$ region), which we consider a lower bound because of uncertainty in $M_c$ for so short a period. The JMA catalog can also supply an estimate of the background rate, after conversion to equivalent KU magnitudes. There were 181 $M_{JMA}\geq 2.2$ shocks in the study area during the 2.5-yr period, October 1994 to March 1997. From the comparison between JMA and KU catalogs (Figure 3b), $M_{JMA} = 0.67 \times M_{KU} + 1.00$. So $M_{JMA}=2.2$ corresponds to $M_{KU}=1.8$. Because $b$=0.9 (Figure 4), $N_{M=0.9} = N_{M=1.8} \times b \times 10^{(1.8-0.9)} = 1438$ earthquakes. The background rate of $M_{KU}\geq 0.9$ would then be 0.3/km$^2$/yr, 3.5 times higher than our more direct estimate based on a briefer period. Since most of this increase is associated with the 1994 rupture zone, this rate is less representative of the region as a whole, and so we consider it an upper bound. We use this range, together with the along-fault aftershock decay for the March and May mainshocks, to estimate the aftershock duration $t_a$=20-100 yr (Figure 10). Although consistent with independent assessments of 23±8 yr for Kobe [*Toda et al.*, 1998] and 35±8 yr for the North Anatolia fault [*Parsons et al.*, 2000], none of these durations are well determined. Since $\dot{\tau}_r = A\sigma/t_a$ [*Dieterich*, 1994], $\dot{\tau}_r$ = 0.004-0.02 bars/yr, a reasonable value given the observed (deviatoric) shear strain rate of 0.10-0.15 x 10$^{-6}$/yr [*Sagiya et al.*, 2000].

*Model comparison with seismicity time series*. Although sensitive to the aftershock duration $t_a$, the rate/state stress transfer model captures the observed time-dependent evolution of seismicity in the selected boxes fairly well (upper panels in Figure 8), and it certainly does better than the stress changes alone (lower panels in Figure 8). In box A, just off the western end of the March rupture, the observed inverse-time decay in seismicity resembles the rate/state model. Box B, just off the south end of the May rupture, was subjected to a 1.2-bar stress increase, and is associated with increase in seismicity rate by more than an order of magnitude. Both the seismicity-rate jump and ensuing decay are fit by the rate/state model with $t_a$ between 20 and 100 yr. Box C is in the trigger zone off the east end of the March rupture, but falls under a stress shadow in May, at which time the observed and modeled seismicity rate drops by 40%.

*Model comparison with spatial distribution of seismicity*. Maps of the predicted number of off-fault earthquakes, constructed from the seismicity rate equation and the calculated Coulomb stress changes (for $\mu$=0.8), are shown in Figure 11. The stress trigger zones appear red because the rate of earthquakes is calculated to exceed the background rate, and the stress shadows appear translucent because the rate of shocks is lower than the background. Note that the plots are not cumulative; each earthquake occurs in only one plot. The time periods are in log time, so that roughly equal numbers of earthquakes occur in each panel.

Many of the off-fault seismicity patterns are reflected in the rate/state model. The lobes of predicted off-fault aftershocks following the March mainshock roughly correspond with the observed seismicity (Figure 11a). The junction of the May faults lies in a lobe of expected off-fault seismicity. This pattern is altered by the May mainshock (Figure 11b), the fault end lobes from the March shock disappearing and a new lobe extending south from the southern end of the May rupture. With time, the new off-fault lobes grow in intensity and migrate away from the fault ruptures, and a memory of the March fault-end lobes also becomes apparent.

The calculations in Figure 11 under-predict the number of shocks in the southern lobe and over-predict the number in the northernmost lobe, perhaps because we use a spatially uniform seismicity background rate. Further, the western off-fault seismicity extends to the south of our predicted location. These misfits are reflected in a spatial regression of the observed on predicted number of earthquakes, in which the along fault seismicity shown in the insets of Figure 10 is excluded. The regression yields $y = 0.74b+0.27$, with a correlation coefficient $\mathbf{r}$=0.27, for 1674 observations measured in 1 km$^2$ bins. Here, $y$ is the observed earthquake density, $b$ is the predicted density, and $\mathbf{r}$ is the regression coefficient (a perfect correlation would yield $y$=1.0$b$+0.0, with $\mathbf{r}$=1.0). Although the regression is significant at the 99.9% confidence level, it explains only a quarter of the variance in the data. For $\mu$=0.0, the observed $\mathbf{r}$=0.20. By comparison, $\mathbf{r}$=0.49 for a study of the 7000 M≥3 earthquakes that struck during the 2000 Izu Islands swarm [*Toda et al.*, 2002].

*Probability of future large shocks*. One can easily transform maps of the expected number of M≥0.9 shocks into the number of earthquakes of any magnitude for any time period, given a magnitude-frequency relation. For large events, in which the expected number

in a period of interest may be less than one, one can calculate the probability of occurrence in addition to the rate. In our case (Figure 4), the rate of M≥5.0 shocks is $2.7 \times 10^{-4}$ times that of M≥0.9 shocks, and the rate of M≥6 shocks is $9 \times 10^{-5}$. For a stationary Poisson process, the probability, $P = 1 - \exp(-N)$, where $N$ is the number of expected events in a time interval and location of interest. In the four triggering lobes, the 10-yr (2004-2014) probability of M≥5 shocks ranges over 35-64%; for M≥6 shocks it is 8-13% (Figure 12). There is a 98% probability of M≥5 (4 shocks expected) and 39% probability of M≥6 (0.5 shocks expected) for the entire area. Because the correlation coefficient of the observed on predicted M≥0.9 seismicity (Figure 11d) is low, the true uncertainty on these probabilities is large, and we offer them as an example rather than a forecast.

Our predicted rate of M≥5 and M≥6 shocks for 2004-2014 is 8-17 times higher than the observed background rate, and all of the increase comes from the trigger zones of Figure 12. Even though there are equal areas of stress increase and decrease, in rate/state stress transfer the exponential response of the seismicity rate to a stress change means that net earthquake rates will be elevated during the aftershock duration. (To gauge the background rates, we use the JMA catalog, which is complete to M=5.0 since 1926, and the Usami catalog, complete to M=6.0 since 1885 [*Earthquake Research Committee*, 1998; *Usami*, 1996]. The rate within the area of Figure 12 is so low that we measure the background rate over a co-located box four times larger, as listed in Table 1).

## 5. Discussion and Conclusion

We provide a roadmap to progress from coseismic slip to stress change, from there to time-dependent seismicity, and finally to earthquake probability. Whether others will want to go down this road remains to be seen. The guiding principle is to use the large sample of small earthquakes to test the predicted temporal and spatial distribution of seismicity predicted by rate/state friction. We have met with some progress in this effort, enough perhaps to warrant additional work, but not enough to claim success.

We benefited from well-recorded, geometrically simple earthquakes that are close enough to interact strongly. But there are nevertheless considerable sources of uncertainty. For the earthquake stress changes (Figure 6), these include the slip model,

the friction coefficient, the depth dependence of stress, and the orientation and rake of the assumed receiver planes. For the density plots (Figure 11), additional uncertainties arise from the rate/state parameters, including the aftershock duration, the constitutive parameter times the normal stress, $A\sigma$, and the assumed uniform background seismicity rate. Finally, for probability forecasts (Figure 12), we further assume that a frequency-magnitude relation derived from the past 5 years applies to the succeeding decade.

Most unequivocally, we show that stress changes can turn on or off seismicity. This is important not only to demonstrate the role of static stress changes, but also to argue that the promotion of seismicity by earthquake shaking effects, or by the dynamic Coulomb stress changes, cannot play a large role in controlling seismicity. The dynamic Coulomb stress changes, while spatially non-uniform, are everywhere positive [*Gomberg et al.*, 2001; *Kilb et al.*, 2000], and thus sudden seismicity rate declines should never be observed. In addition, the dynamic Coulomb stresses are greatest in the direction of rupture propagation. The March rupture was bilateral and so these effects should be similar beyond both fault ends, but instead off-fault seismicity is much more vigorous to the west (Figure 11d). The May shock ruptured unilaterally to the east and south. Yet there is no eastern off-fault seismicity, a feature we attribute the static stresses imposed by the March event (Figure 11b-d). What we do not reproduce in any of these calculations is the along-fault seismicity, which we believe arises from stress and geometrical discontinuities that are not included in our smooth slip model. Our ability to consider these shocks must await higher-resolution of variable-slip source models, but these will surely come.

We have argued that the final state of seismicity cannot be calculated by adding the stress contributed by a sequence of earthquakes for two reasons: According to the theory of rate/state friction, the effect of stress on seismicity fades with time, and the stress changes amplify (if positive) or suppress (if negative) the background seismicity rates. In this context, 'background' is not the long-term average, but the rate of seismicity immediately before a stress change occurs. If, for example, the stress drops at a site because of one earthquake, a second stress increase will have a much smaller effect on seismicity rates than if the first earthquake had not occurred. The theory exhibits a rough match to the distribution, temporal evolution, and apparent migration of the off-fault seismicity at Kagoshima. We found that stress trigger zones enhance seismicity and stress shadows inhibit earthquake occurrence. As the observation period approaches the

aftershock duration, both the lobes and shadows will fade, but the trigger zones will have produced many more shocks than are missing from the shadows.

**Acknowledgements.** We thank Gerald Bawden for analyzing the GPS data for us; Kazuhiko Goto and Hiroki Miyamachi for sharing their seismic data and analyses; and Haruo Horikawa for discussing his slip inversion. We are very grateful to Wayne Thatcher and Jeanne Hardebeck for perceptive reviews.

## References

Belardinelli, M.E., M. Cocco, C. O., and F. Cotton, Redistribution of dynamic stress during coseismic ruptures: Evidence for fault interaction and earthquake triggering, *J. Geophys. Res.*, *104*, 14,925-14,945, 1999.

Dieterich, J., A constitutive law for rate of earthquake production and its application to earthquake clustering, *J. Geophys. Res.*, *99*, 2601-2618, 1994.

Earthquake Research Committee, *Seismic activity in Japan: Regional perspectives on the characteristics of destructive earthquakes*, 222 pp., Science and Technology Agency, Tokyo, 1998.

Fujiwara, S., H. Yarai, S. Ozawa, M. Tobita, M. Murakami, H. Nakagawa, and K. Nitta, Surface displacement of the March 26, 1997 Kagoshima-ken-hokuseibu earthquake in Japan from synthetic aperture radar interferometry, *Geophys. Res. Lett.*, *25*, 4541-4544, 1998.

Gomberg, J., P.A. Reasenberg, P. Bodin, and R.A. Harris, Earthquake triggering by seismic waves following the Landers and Hector Mine earthquakes, *Nature*, *411*, 462-466, 2001.

Guatteri, M., P. Spudich, and G.C. Beroza, Inferring rate and state friction parameters from a rupture model of the 1995 Hyogo-ken Nanbu (Kobe) Japan earthquake, *J. Geophys. Res.*, *106.*, 26,511-26,521, 2001.

Harris, R.A., and R.W. Simpson, Suppression of large earthquakes by stress shadows: A comparison of Coulomb and rate-and-state, *J. Geophys. Res.*, *103*, 24,439-24,451, 1998.

Horikawa, H., Earthquake doublet in Kagoshima, Japan; rupture of asperities in a stress shadow, *Bull. Seismol. Soc. Amer.*, *91*, 112-127, 2001.

Hubert-Ferrari, A., A. Barka, E. Jacques, S.S. Nalbant, B. Meyer, R. Armijo, P. Tapponnier, and G.C.P. King, Seismic hazard in the Marmara Sea region following the 17 August 1999 Izmit earthquake, *Nature*, *404*, 269-273, 2000.

Kilb, D., J. Gomberg, and P. Bodin, Earthquake triggering by dynamic stresses, *Nature*, *408*, 570-574, 2000.

Marone, C., Stressed to a quaking point, *Nature*, *419*, 32, 2002.

Matthews, M.V., and P.A. Reasenberg, Statistical methods for investigating quiescence and other temporal seismicity patterns, *Pure and Appl. Geophys.*, *126*, 357-372, 1988.

Miyake, H., T. Iwata, and K. Irikura, Strong motion simulation and source modeling of the Kagoshima-ken Hokuseibu earthquakes of March 26 ($M_{JMA}$ 6.5) and May 13 ($M_{JMA}$ 6.3), using empirical Green's function method, *Zisin*, *51*, 431-442, 1999.

Miyamachi, H., K. Iwakiri, H. Yakiwara, K. Goto, and T. Kakuta, Fine structure of aftershock distribution of the 1997 Northwestern Kagoshima earthquakes with a three-dimensional velocity model, *Earth, Planets and Space*, *51*, 233-246, 1999.

Nalbant, S.S., A. Hubert, and G.C.P. King, Stress coupling between earthquakes in northwest Turkey and the north Aegean sea, *J. Geophys. Res.*, *103*, 24,469-24,486, 1998.

NIED staff, Seismic Moment Tensor Catalogue, *Technical Note of the National Research Institute for Earth Science and Disaster Prevention*, *205-218*, 2001.

Parsons, T., R.S. Stein, R.W. Simpson, and P.A. Reasenberg, Stress sensitivity of fault seismicity: A comparison between limited-offset oblique and major strike-slip faults, *J. Geophys. Res.*, *104*, 20,183-20,202, 1999.

Parsons, T., S. Toda, R.S. Stein, A. Barka, and J.H. Dieterich, Heightened odds of large earthquakes near Istanbul: An interaction-based probability calculation, *Science*, *288*, 661-665, 2000.

Reasenberg, P.A., and R.W. Simpson, Response of regional seismicity to the static stress change produced by the Loma Prieta earthquake, *U.S. Geol. Surv. Prof. Pap.*, *1550-D*, 49-72, 1997.

Sagiya, T., S. Miyazaki, and T. Tada, Continuous GPS array and present-day crustal deformation of Japan, *Pure Appl. Geophys.*, *157*, 2303-2322, 2000.

Stein, R.S., The role of stress transfer in earthquake occurrence, *Nature*, *402*, 605-609, 1999.

Stein, R.S., A.A. Barka, and J.H. Dieterich, Progressive failure on the North Anatolian fault since 1939 by earthquake stress triggering, *Geophys. J. Int.*, *128*, 594-604, 1997.

Toda, S., and R.S. Stein, Response of the San Andreas fault to the 1983 Coalinga-Nuñez Earthquakes: An application of interaction-based probabilities for Parkfield, *J. Geophys. Res.*, *107*, 10.1029/2001JB000172, 2002.

Toda, S., R.S. Stein, P.A. Reasenberg, and J.H. Dieterich, Stress transferred by the $M_w$=6.5 Kobe, Japan, shock: Effect on aftershocks and future earthquake probabilities, *J. Geophys. Res.*, *103*, 24,543-24,565, 1998.

Toda, S., R.S. Stein, and T. Sagiya, Evidence from the A.D. 2000 Izu Islands swarm that seismicity is governed by stressing rate, *Nature*, *419*, 58-61, 2002.

Usami, T., *Materials for comprehensive list of destructive earthquakes in Japan (revised and enlarged edition)*, 493 pp., Univ. Tokyo Press, Tokyo, 1996.

Wiemer, S., A software package to analyse seismicity: ZMAP, *Seismol. Res. Letts.*, *72*, 373-382, 2001.

Wiemer, S., and M. Wyss, Minimum magnitude of completeness in earthquake catalogs: Examples form Alaska, the western United States, and Japan, *Bull. Seismol. Soc. Amer.*, *90*, 859-869, 2000.

Wyss, M., and S. Wiemer, Change in the probability for earthquakes in southern California due to the Landers Magnitude 7.3 earthquake, *Science*, *290*, 1334-1338, 2000.

Table 1. Background earthquake rate in the Kagoshima region before May 1997

| Earthquake magnitude | Time period for complete catalog | Observed number of shocks | Rate per decade per $km^2$ | Background rate per decade for area of Fig. 12 | Predicted for decade, 2004-20014 |
|---|---|---|---|---|---|
| M≥5 | 1926-1997 | 7 | $1.25 \times 10^{-4}$ | 0.23 | 4 |
| M≥6 | 1885-1997 | 3 | $3.42 \times 10^{-5}$ | 0.06 | 0.5 |

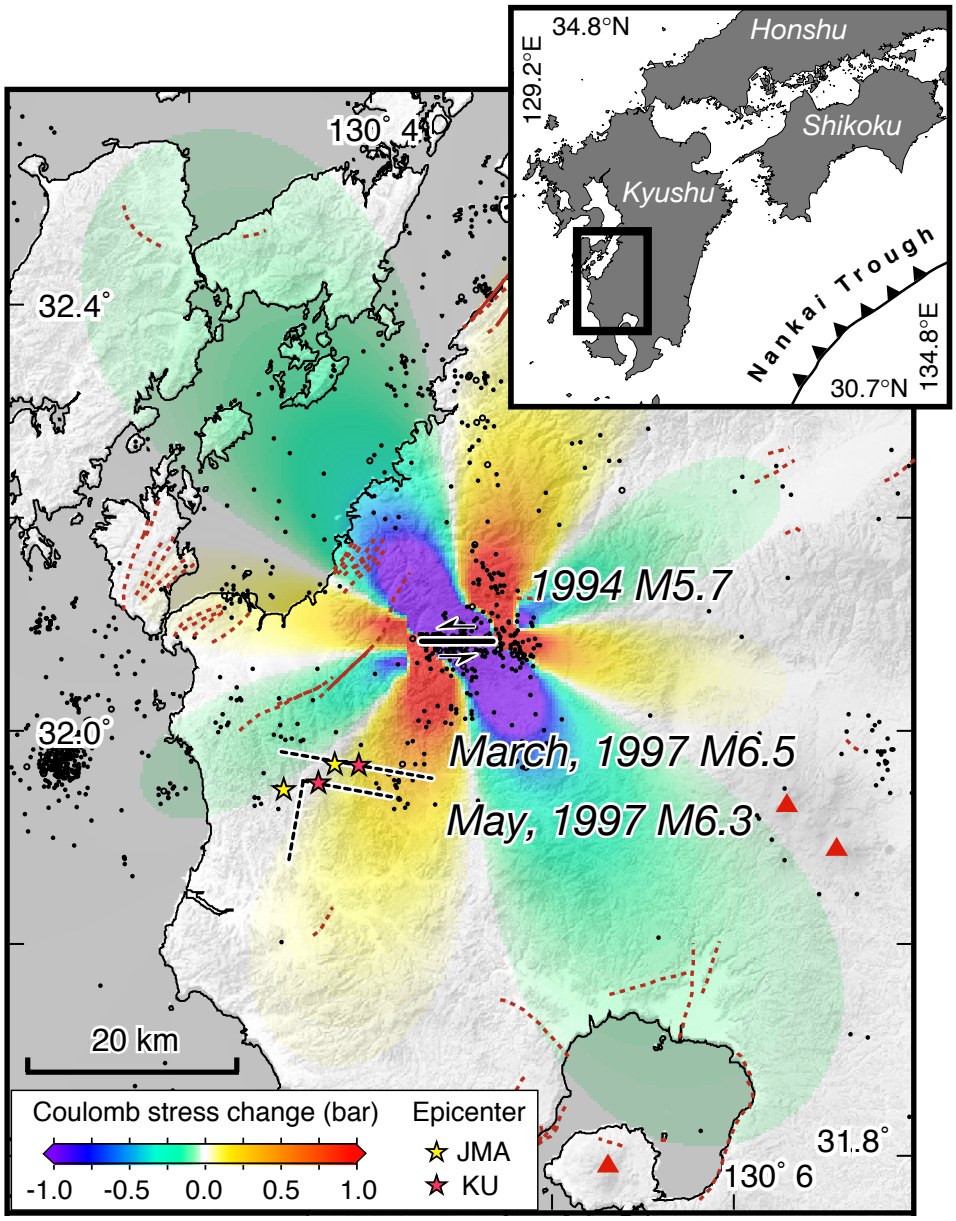


**Figure 1** Site of the 1997 Kagoshima earthquake sequence (dashed black lines) in southwest Japan, with January 1990-February 1997 JMA M≥2.2 seismicity shown. Active faults are red (dashed where inferred); active volcanoes are red triangles [*Earthquake Research Committee*, 1998]. The Coulomb stresses (for a friction coefficient, μ=0.8) imparted by the 13 February 1994 $M_{JMA}$=5.7 shock, adopting its Harvard CMT solution (**M**=5.4, strike=89°, dip=89°, rake=-1°, lat/lon=32.03°/130.33°, with a 7.3 x 7.3-km patch with 0.28 m of slip) is superimposed. For μ=0.4, failure is promoted by 0.25 bars only on the east half of the March 1997 fault.

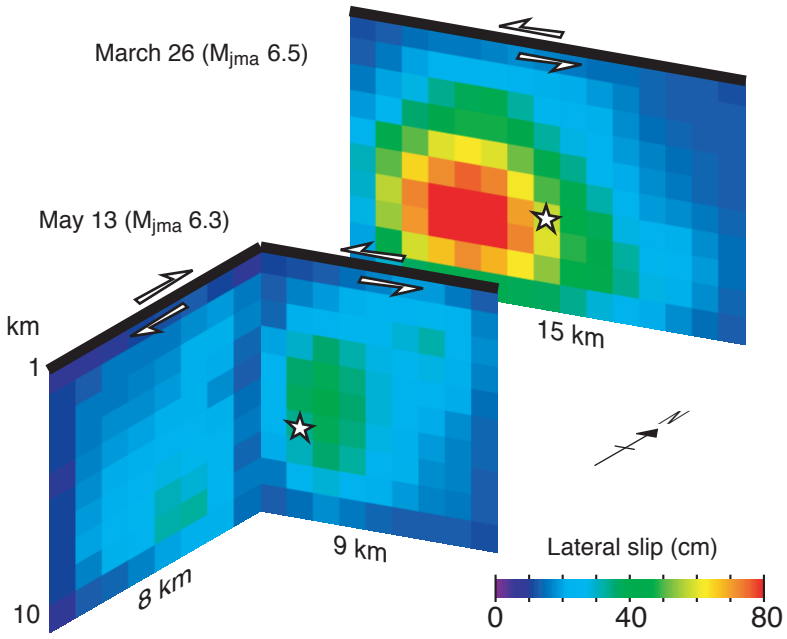


**Figure 2** Variable slip model of *Horikawa* [2001] for the couplet. The March and May sources have been separated to make the March slip visible in this perspective.

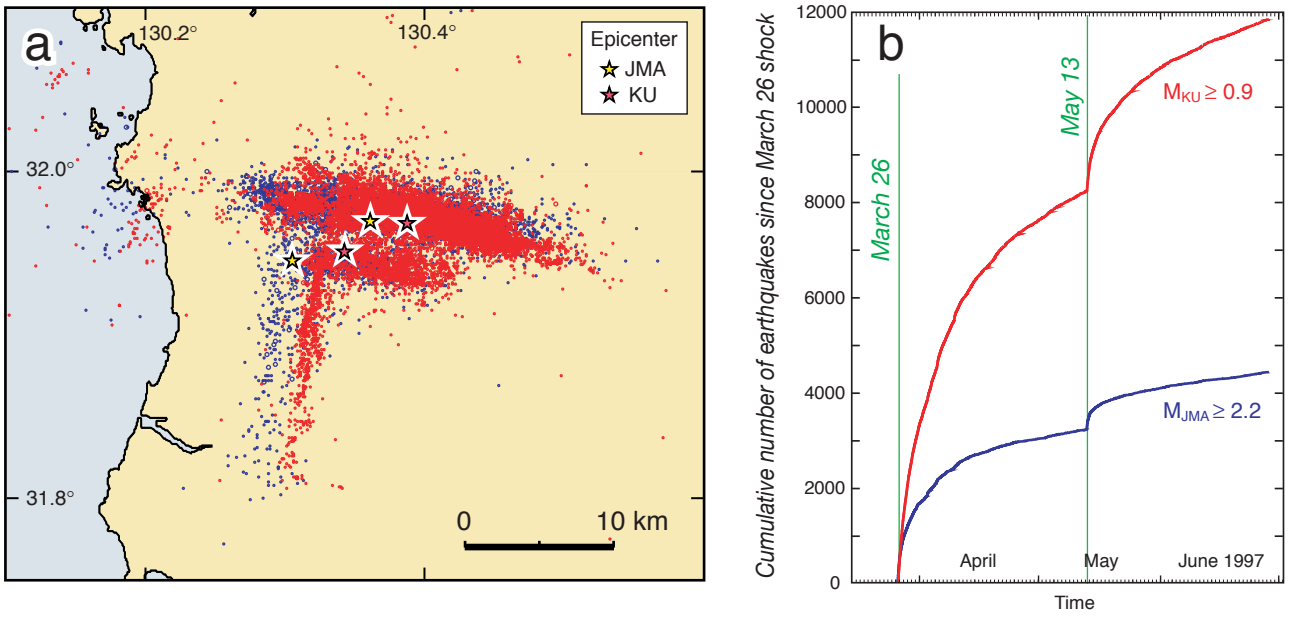


**Figure 3** (a) Seismicity during the 96-day period starting March 26 from the JMA (blue) and Kagoshima University (red) catalogs. The JMA mainshocks are blue and Kagoshima University shocks are pink. (b) Cumulative number of earthquakes as a function of time, at the magnitude of completeness, for the JMA and Kagoshima University catalogs for the 96-day period starting March 26. Note as well a systematic 2.5-km eastward locations of the Kagoshima University to JMA seismicity.

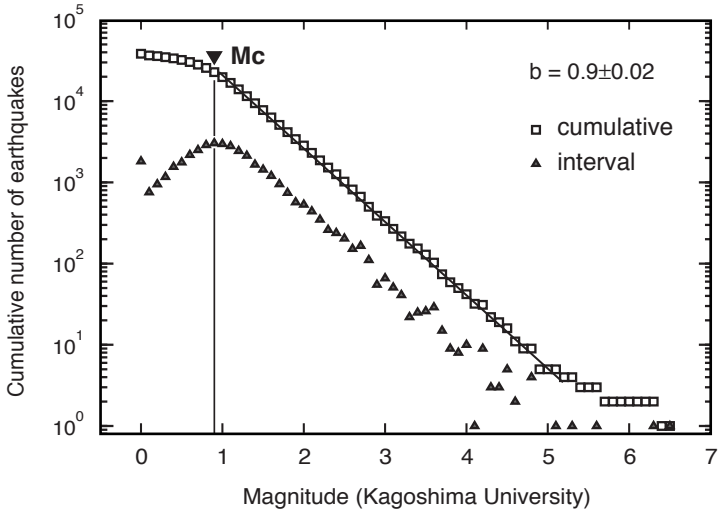


**Figure 4** Maximum likelihood solution for the minimum magnitude of completeness, $M_c$, for the Kagoshima University catalog for March 1996-March 2001, calculated using ZMAP of *Wiemer* [2001]. The b-value is for 0.9≥M≥5.0.

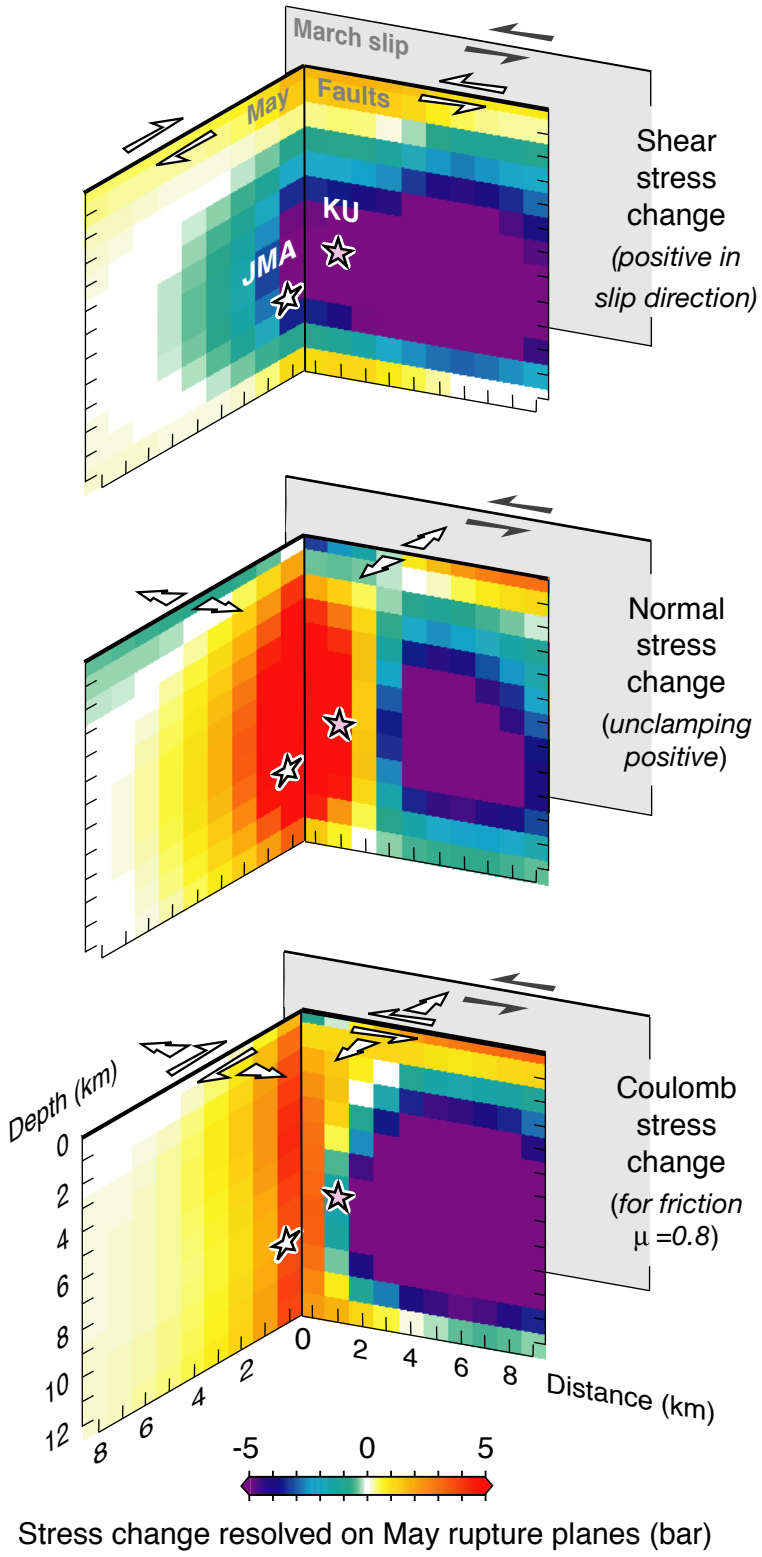


**Figure 5** Perspective view of stress imparted by the March mainshock resolved on the planes that ruptured in May. Slip is represented by the black arrows; stress by the white arrows. Whether the May event was triggered by the static stress changes is dependent upon the assumed friction coefficient and the location of the May hypocenter (KU, Kagoshima University location; JMA, Japan Meteorological Agency location).

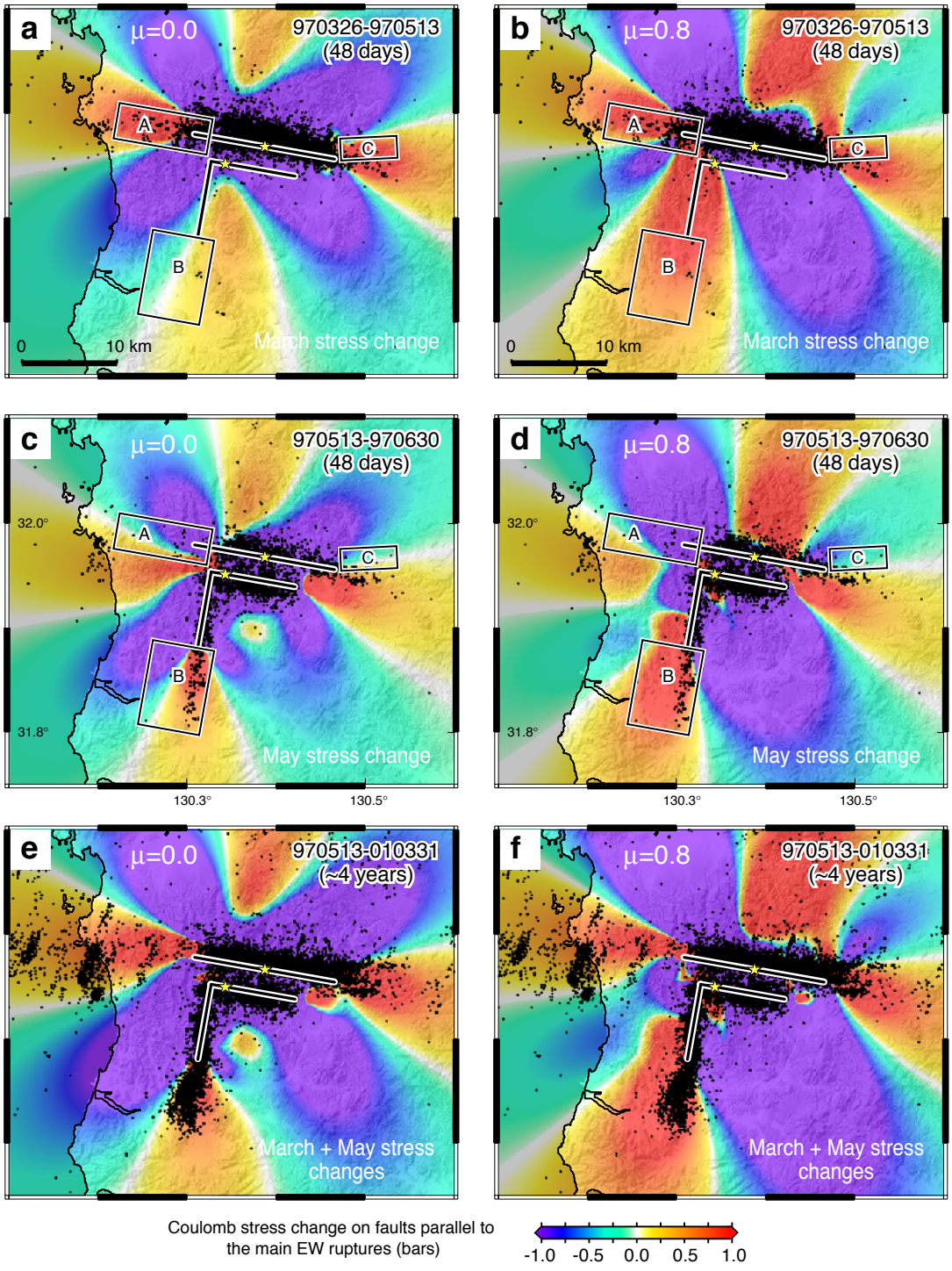


**Figure 6** Aftershocks from the Kagoshima University catalog relocated by *Miyamachi et al.* [1999] superimposed on coseismic stress changes at 5 km depth for the March (a-b) and May (c-d) mainshocks; both are 48-day periods. Also shown are boxes for the seismicity time series plotted in Figure 8. The combined stress changes and the full 4 years of post-May 13 shocks are shown in (e-f).

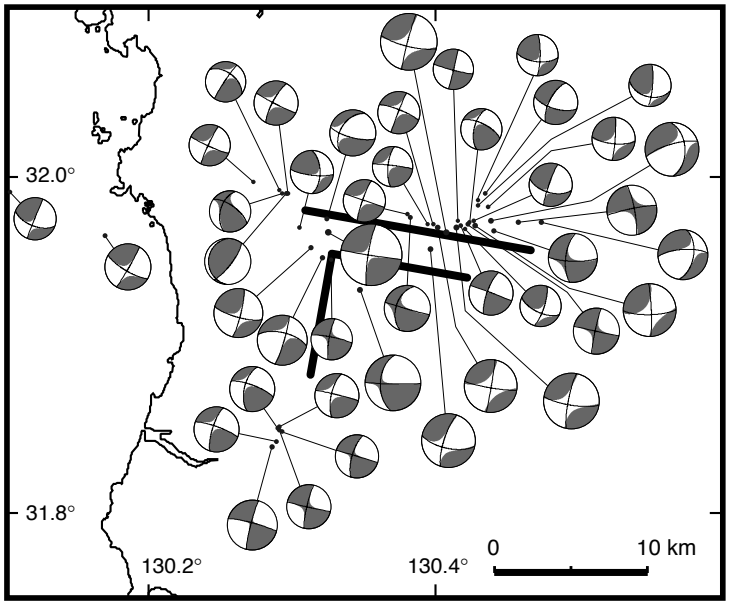


**Figure 7** All well-determined focal mechanisms for M≥3 shocks, as determined by the F-net broadband network during March 1997 to March 2001 [*NIED staff*, 2001]. The majority of both on-fault and off-fault shocks exhibit nodal planes parallel to the rupture planes of the main ruptures.

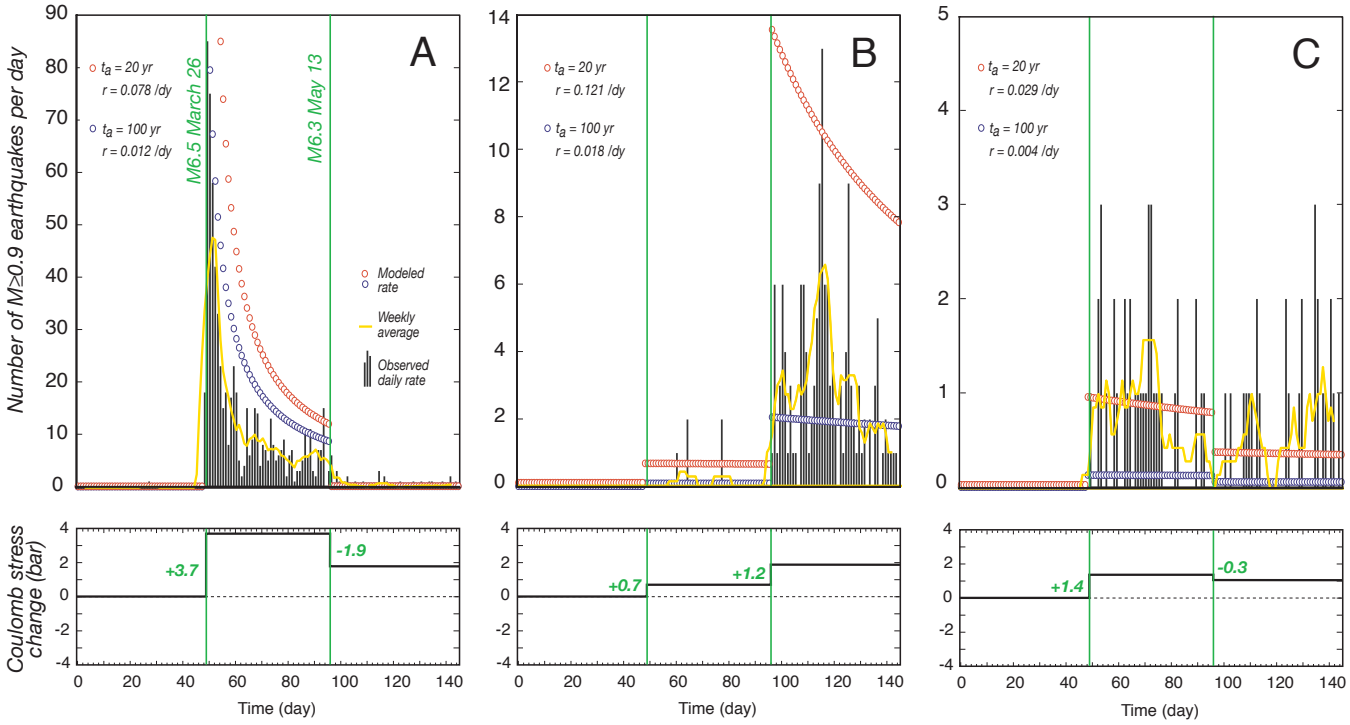


Figure 8 Observed and modeled seismicity time series for the boxed regions shown in Figure 6. Running weekly average seismicity rates are yellow. Note that the seismicity-rate scale in the upper panels differs for each box. Shown below each time series is the calculated Coulomb stress history for μ=0.8. The background rates used to calculate the expected seismicity evolution vary as a function of box size; the estimated rate is $2.5 \times 10^{-4}$ km$^{-2}$ dy$^{-1}$. The range in aftershock duration $t_a$ is shown in Figure 10.

Seismicity rate of *Dieterich* [1994]

$$R_n = \frac{r}{\gamma_n \dot{\tau}_r}$$

*Steady state* (initial state variable)

$$\gamma_o = \frac{1}{\dot{\tau}_r} \quad (1)$$

*Jump* (evolution at a new stress step)

$$\gamma_n = \gamma_{n-1} \exp\left(\frac{-\Delta\tau}{A\sigma}\right) \quad (2)$$

*Decay* (evolution with time after a stress step)

$$\gamma_{n+1} = \left[\gamma_n - \frac{1}{\dot{\tau}_r}\right] \exp\left[\frac{-\Delta t\ \dot{\tau}_r}{A\sigma}\right] + \frac{1}{\dot{\tau}_r} \quad (3)$$

| | | | |
|---|---|---|---|
| $\dot{\tau}_r$ | secular shear stressing rate | $\Delta t$ | time increment used to recalculate $\gamma$ |
| $r$ | background seismicity rate | $A\sigma$ | constitutive parameter times the normal stress |
| $\gamma_n$ | state variable ($n$ time steps) | $\Delta\tau$ | Coulomb stress change |
| $\gamma_o$ | state variable at steady state | | |

**Figure 9** Seismicity rate equation of *Dieterich* [1994], showing how the state variable evolves with each earthquake stress change and the intervening decay.

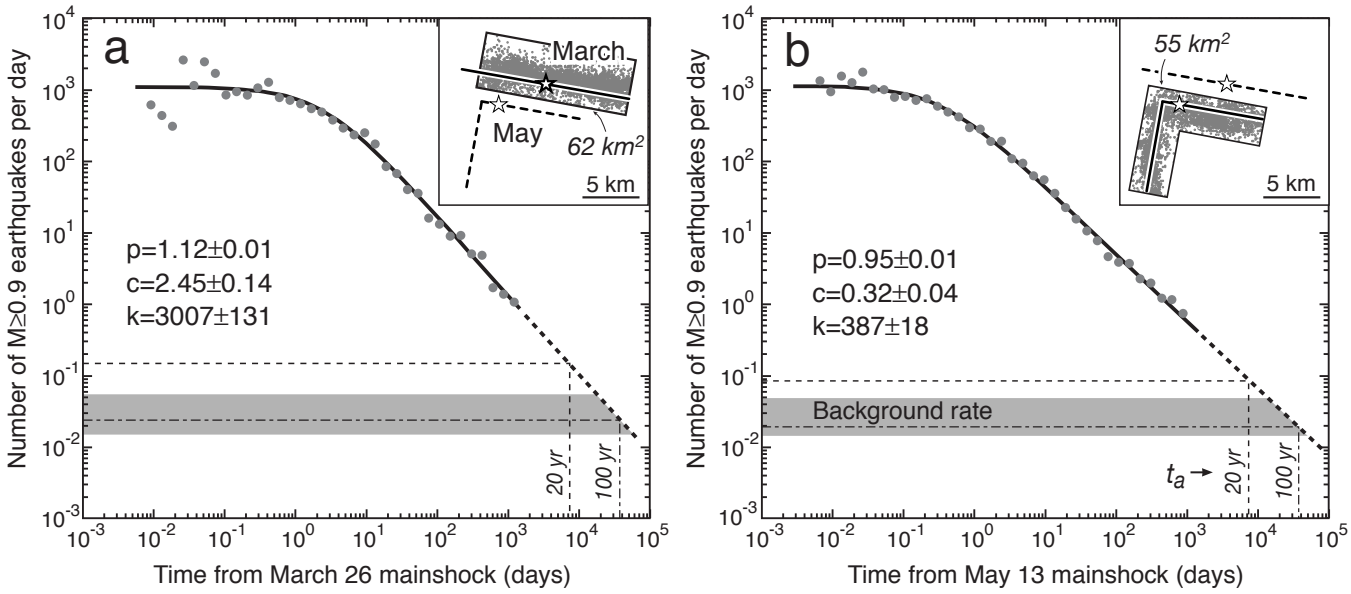


**Figure 10** Observed aftershock rate (dots) as a function of time for the March 26 and May 13 shocks, fitted (line) to a modified Omori decay function, $N(t)=k/(t+c)^p$. Aftershocks and the associated fault ruptures are shown in the inset maps, and the bounds on the estimated background rate are shown gray horizontal bands. The lower bound comes from the 1996 rate in the KU catalog; the upper bound is from the 1994-1996 rate in the JMA catalog, after conversion to equivalent KU magnitudes. The inferred aftershock duration $t_a$ corresponds to the time when the projected aftershock rate (heavy dashed line) decays to the background rate.

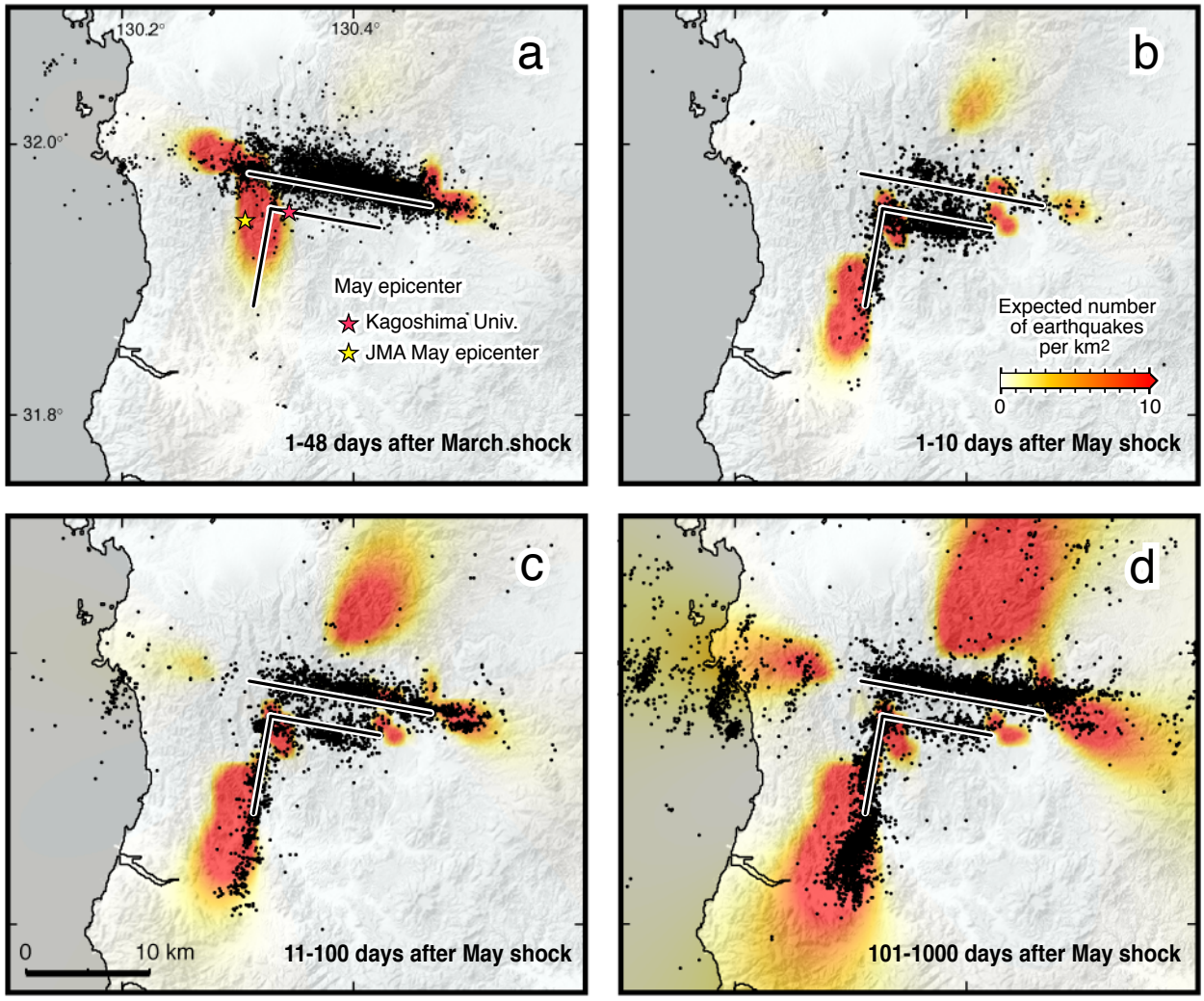


**Figure 11** Observed seismicity in bins of increasing time, superimposed on the number of earthquakes calculated by rate/state stress transfer (for μ=0.8). Stress trigger zones appear as warm tones; stress shadows as translucent. Increasing time periods after the May shock are used for (b-d). Since the first period is truncated 48 days later by the May shock, the full 48-day interval is shown in (a).

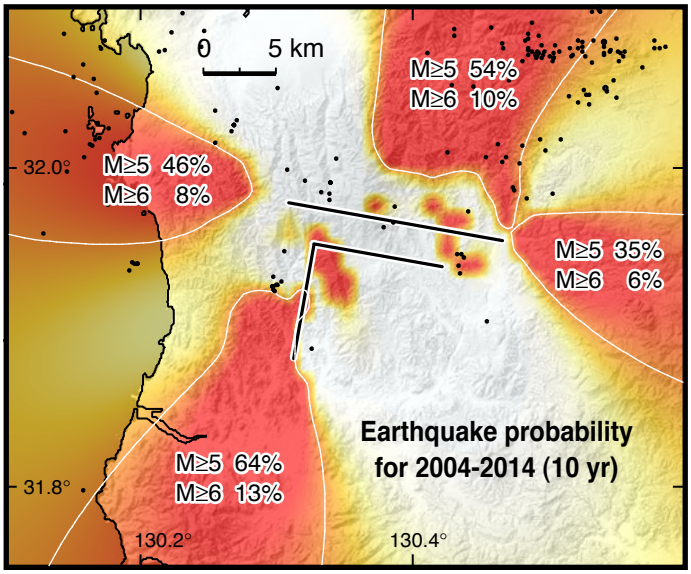


**Figure 12** Probability of M≥5 and M≥6 shocks in the vicinity of the 1997 Kagoshima earthquake sequence, for the decade, 2004-2014, assuming Aσ=0.4 bar and $t_a$=20 yr. Probabilities correspond to the areas inscribed by the white lines.